Thermoelastic Modeling of Layered Composites Considering Bending and Shearing Effects

Yanchu Zhang[1]; Qiliang Lin[2]; and Huiming Yin[3]

Abstract: Composite materials and structures often exhibit thermal stresses and deformations due to their thermal expansion mismatch. For a layered laminate, the stress transfer mechanism involves both bending and interfacial shearing, which have been evaluated by Stoney's equation and shear lag models, respectively. However, the two theories cannot consider both effects simultaneously due to their distinct assumptions. Because bending and shearing effects coexist in the physical problem, higher accuracy and fidelity can be achieved by considering both mechanisms. This paper presents an analytical formulation to solve this boundary value problem by constructing two separate trial functions from Navier's equation. The analytical solution was proposed with an assumption of a perfectly bonded interface, and the corresponding coefficients were determined with the principle of stationary potential energy. The proposed model was applied to thermomechanical analysis of thin-film photovoltaic cells on smart window blinds, and good agreement was achieved between the theoretical prediction and finite-element results. A parametric study was also conducted to guide the design of solar window blinds and general bilayered composites. **DOI: 10.1061/(ASCE)EM.1943-7889.0001943.**

Introduction

Layered materials have been widely observed in the natural world and extensively used in the industry for their versatile applications, such as sound absorption panels (Lee et al. 2005; Zulkifli et al. 2008), stretchable electronics (Guo and DeWeerth 2010; MacDonald et al. 2007), and laminated composites (Anbusagar et al. 2015; Hou et al. 2015). As an important application of layered structures, solar panels involve multiple layers with different components and are widely applied to convert solar energy to electricity (Sumitomo et al. 2011; Yang et al. 2012; Yin et al. 2013). Thanks to the rapid development in material science and advances in semiconductor manufacturing in the recent decade, the quality and thickness of photovoltaic (PV) cells have witnessed a significant improvement, contributing to their wide application in different regions (Razeghi 2002). The application of thin-film PV cells requires a comprehensive understanding of their layered structure, especially thermomechanical performance under a static temperature change so that the potential cracks and failures can be avoided under proper design and engineering. Although the absolute difference of the thermal expansion coefficients appears insignificant, that is, 8.8×10^{-6} K^{-1} of glass substrate (Roy et al. 1989) versus 3.6×10^{-6} K^{-1} of a silicon cell (Yim and Paff 1974), irreversible damage in this brittle material system, including microcrack initiation and inelastic deformation, could occur as a consequence of thermal cycling.

Recently, an innovative smart window system was designed with PV-integrated blinds and is schematically shown in Fig. 1(a) (Lin et al. 2020). The blinds were manufactured by attaching the PV cells to a transparent glass substrate for solar energy harvesting. Solar window blinds are typically made of layered structures similar to the layout of PV panels, such as the glass-cell-glass (GCG) design in Fig. 1(b) or the glass-cell-Tedlar (GCT) design in Fig. 1(c). In both design schemes, ethylene-vinyl acetate (EVA) is selected as an adhesive to bond the layers. Because the Tedlar and EVA are considered nonmechanical layers due to their negligible stiffness compared to glass, the models can be simplified into a glass substrate and PV cell overlay with a fully bonded interface. Therefore, the following discussion will focus on the GCG and GCT models, in which only two material phases are involved. Considering geometric and material properties, the GCT system shows curvature under thermal loads, whereas the GCG system remains flat due to symmetry.

To interpret residual stress transfer and distribution in an overlay-substrate structure, Stoney proposed a theory that assumed a uniform uniaxial residual stress in the overlay (Stoney 1909). This theory could be applied to situations where a thin film layer is deposited on a thick substrate so that the bending stiffness of the thin film is ignored, and thus the residual stress is distributed uniformly. Some experiments have successfully validated the accuracy of Stoney's equation in ferroelastic materials (Corkovic et al. 2008) and micro-electromechanical system (MEMS) (Huang and Zhang 2006) by measuring the curvature with techniques including X-ray tomography and the laser curvature method (Zhao et al. 2002). The accuracy of Stoney's equation was further improved for thick overlays undergoing a large deformation by considering the strain energy from both overlay and substrate (Freund et al. 1999). Because shear transfer through the interface was not considered in Stoney's equation, it cannot explain the interfacial sliding between layers and shear stress distribution. A modified theory was developed with the assumption that the shear stress was distributed as a piecewise constant function to account for sliding between interfaces (Haftbaradaran et al. 2012). This modified theory was extended to a multidimensional model for thin film islands by solving the governing equations in polar coordinates with

[1]Graduate Research Assistant, Dept. of Civil Engineering and Engineering Mechanics, Columbia Univ., 610 Seeley W. Mudd, 500 West 120th St., New York, NY 10027. Email: yz3473@columbia.edu

[2]Postdoctoral Research Scientist, Dept. of Civil Engineering and Engineering Mechanics, Columbia Univ., 610 Seeley W. Mudd, 500 West 120th St., New York, NY 10027. Email: ql2241@columbia.edu

[3]Associate Professor, Dept. of Civil Engineering and Engineering Mechanics, Columbia Univ., 610 Seeley W. Mudd, 500 West 120th St., New York, NY 10027 (corresponding author). ORCID: https://orcid.org/0000-0001-6549-9066. Email: yin@civil.columbia.edu

Note. This manuscript was submitted on July 1, 2020; approved on February 17, 2021; published online on April 26, 2021. Discussion period open until September 26, 2021; separate discussions must be submitted for individual papers. This paper is part of the ***Journal of Engineering Mechanics***, © ASCE, ISSN 0733-9399.

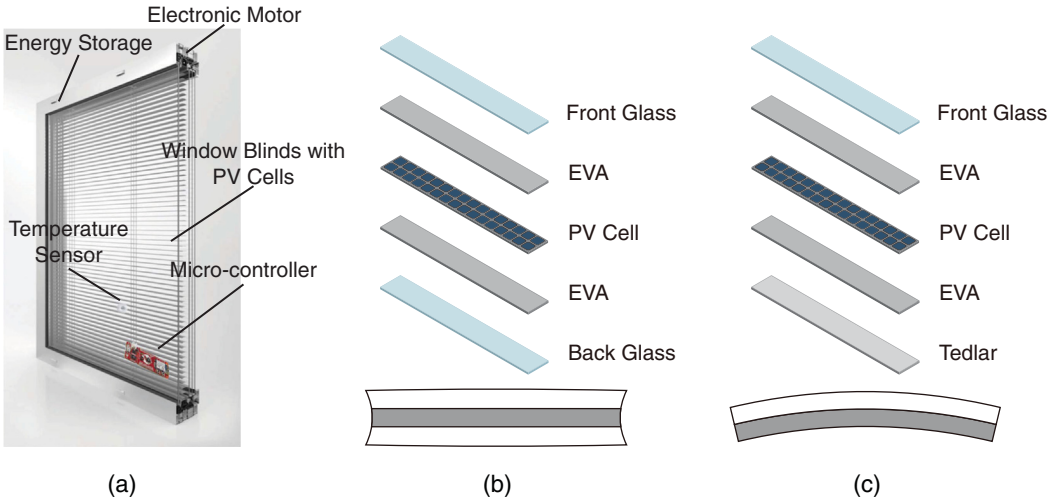

Fig. 1. Schematic illustration of a solar window blinds system: (a) application of solar window blinds; (b) layout and deformation pattern of GCG solar panel; and (c) layout and deformation pattern of GCT solar panel.

Betti's reciprocity theorem. Stoney's equation, together with other modified theories, received extensive attention and recognition during the last decades, whereas shear stress distribution was not derived rigorously in these theories and needed further investigation. The beam theory assumption that plane sections remain plane may be invalid in some configurations. Particularly for the configuration of GCG in Fig. 1(b), because of symmetry along the thickness, no bending occurs, and thus Stoney's equation is not applicable.

In order to study shear stress transfer in layered structures, some other theories have emerged with specific assumptions. The one-dimensional theory developed by Timm et al. (2003) revealed that the horizontal displacement pattern was an exponential function with a linear frictional interface. However, it ignored the shear lag across the section and thus could not address the stress and displacement distributions along the depth direction. In the two-dimensional case, the stress fields in a thick-wall structure were obtained in polar coordinates and solved with axial symmetry (Feng et al. 2006). The breakthrough of stress distribution in rectangular coordinates was achieved afterward by solving Navier's equations (Yin et al. 2007). This model, which assumed a linear frictional interface to correlate shear stress with displacement proportionally, was used to explain the stress distribution and crack patterns in the pavement design. Among the models mentioned previously, interfacial shear stress was described by an interfacial shear spring (Bogy 1968). However, the shear spring coefficient was implicit and complicated to calibrate. Therefore, a fully bonded bimaterial model was developed based on interfacial continuity conditions in lieu of the calibrated spring constant (Yin et al. 2013). Some researchers subsequently improved the accuracy of the fully bonded model by exploiting Beltrami–Michell stress compatibility as governing equations (Li et al. 2018). Based on the previous well-established theories, the linear elastic problem was extended to viscoelastic analysis to explain the time-dependent property of asphalt (Prieto-Muñoz et al. 2013) and elastoplastic analysis for ductile materials (Chen et al. 2015). All the models mentioned previously can be categorized as shear lag models, where the plane parallel to the longitudinal direction remains plane during shear sliding. The previously mentioned shear lag models can evaluate shear mechanisms in GCG but could not fully capture the bending effect in GCT. However, the shear lag models mentioned previously cannot capture the bending effect in GCT. Models that consider both bending and shear effects have rarely been discussed in the last decades. An approximate model was established in 1988 based on interfacial equilibrium conditions but did not capture the in-depth shear lag effect that happens in GCG (Suhir 1988). Therefore, a profound explanation of the stress transfer mechanism is still underway.

In this paper, a more accurate formulation was proposed to address both bending and shear lag simultaneously. A boundary value problem was formulated for the GCT layout panels as a bilayered structure. General solutions in terms of displacements were derived with two trial functions featuring pure bending and shear transfer. Interfacial compliance parameters were determined through boundary and interfacial continuity conditions. The unknown coefficients of two trial functions were calculated with the aid of the principle of stationary potential energy so that closed-form solutions were obtained by combining two separate trial functions into a complete equation. The proposed method was compared with Stoney's theory, the shear lag model, and the finite-element method (FEM), where a clear improvement of accuracy was observed compared with other theoretical models. In addition, the proposed model also provides a theoretical perspective to explain the combination of bending and shear lag and the thermomechanical behavior of bilayered composites.

The remainder of this paper is organized as follows. The "Formulation" section discusses the assumptions and formulations under the plane stress condition. The elastic solutions for this boundary value problem were obtained with the aid of variational principles. The "Numerical Verification" section demonstrates the accuracy of the proposed model by comparing the theoretical results with the FEM results from ABAQUS and other analytical models in the literature. A parametric study is described in the "Discussion and Parametric Analysis" section to analyze the effect of the material stiffness and layer depth on the thermomechanical properties of the overlay–substrate system, including the displacement and stress fields. The "Conclusions" section summarizes the paper with conclusive remarks.

Formulation

Problem Statement

In GCT layout modeling, glass and PV cells are considered mechanically effective, whereas the adhesives and coatings are neglected. A model with length 2λ, depth h_i, Young's modulus E_i, Poisson's

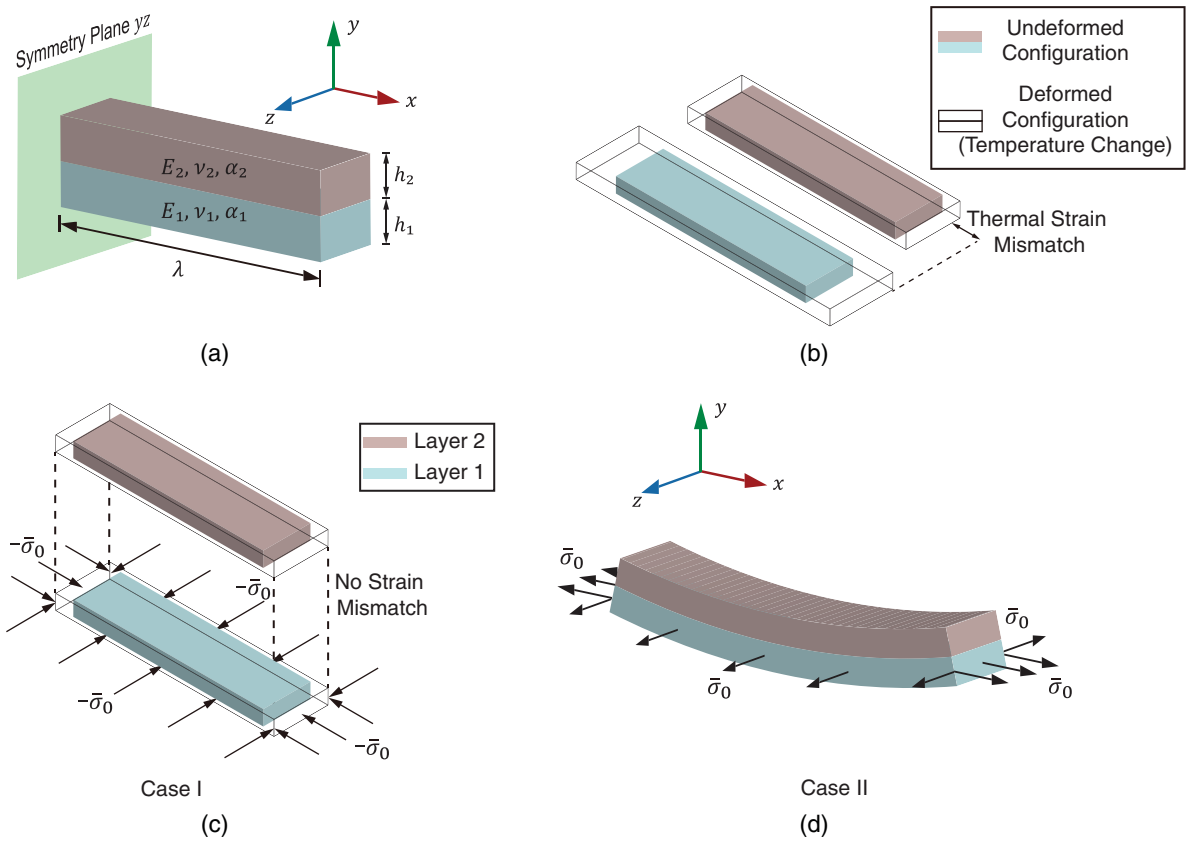

Fig. 2. Diagram of the layered structure: (a) schematic illustration of the thermomechanical model; (b) illustration of thermal strain mismatch; (c) free body diagram in Case I; and (d) free body diagram in Case II.

ratios ν_i, and thermal expansion coefficient α_i was considered in the analysis, where the index $(i = 1, 2)$ indicates the numbering of the layers. By taking advantage of symmetry in the yz plane, the original model was simplified to half of the geometry and is shown in Fig. 2(a). The original thermomechanical problem induced by a temperature change ΔT was decomposed into two mechanical problems, as indicated in Figs. 2(c and d), which is elucidated as follows (Yang et al. 2013):

- In Case I, a virtual biaxial mechanical load $-\bar{\sigma}_0$ was applied at the bottom layer to eliminate the strain mismatch resulting from the difference of thermal expansion coefficients between layers. The minus sign was intentionally introduced for the convenience of the derivation in Case II, and
- In Case II, another virtual load $\bar{\sigma}_0$ in the reverse direction was applied to the bottom layer so that the superposition of the two cases represents the original problem.

In Case I, the deformation compatibility requires the same deformation of the overlay and substrate so that the mechanical load $\bar{\sigma}_0$ can be fully determined through the constitutive equation as follows:

$$\bar{\sigma}_0 = \frac{E_1(\alpha_1 - \alpha_2)\Delta T}{1 - \nu_1} \tag{1}$$

In Case II, the biaxial stress $\bar{\sigma}_0$ is considered as a superposition of two tension problems in the x-direction and z-direction. Because the length in the x-direction is much longer and dominates the mechanical behavior, the structure undergoes a bending deflection due to the eccentric mismatch stress $\bar{\sigma}_0$ along the x-direction. As for the mismatch stress $\bar{\sigma}_0$ in the z-direction, although its effect on the deformation in the z-direction is not the focus and thus disregarded,

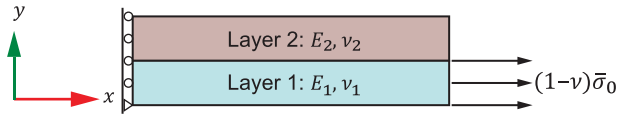

Fig. 3. Schematic illustration of the plane stress bilayered model.

Poisson's effect may produce deformation in the x-direction, which can be equivalently replaced by the stress $-\nu_1\bar{\sigma}_0$ in the x-direction. Therefore, this three-dimensional (3D) thermomechanical problem was simplified to a plane stress model with a reduced mismatch stress $(1 - \nu_1)\bar{\sigma}_0$ to account for the biaxial state. The schematic illustration of the proposed model is illustrated in Fig. 3.

For the GCG layout in Fig. 1(b), the same procedure can be applied using symmetry in the y-direction. Therefore, only half of the PV cell layer was considered, with a symmetry boundary condition at the bottom, that is, $u_y = 0$ and $\sigma_{yx} = \sigma_{yz} = 0$, which eliminated the bending effect. On the contrary, GCT exhibits a free boundary condition at the bottom, and the bending should not be neglected.

Derivation of Trial Functions

The elastic problem in Case II can be described by Navier's equation for a plane stress problem, as

$$\begin{aligned} &\frac{1}{1-\nu^2}u_{x,xx} + \frac{1}{2(1+\nu)}u_{x,yy} + \frac{1}{2(1-\nu)}u_{y,xy} = 0 \\ &\frac{1}{2(1-\nu)}u_{x,xy} + \frac{1}{2(1+\nu)}u_{y,xx} + \frac{1}{1-\nu^2}u_{y,yy} = 0 \end{aligned} \tag{2}$$

where the displacement and stress boundary conditions are written as

$$u_x(0,y)=0$$
$$u_y(0,0)=0 \tag{3}$$

$$\sigma_{xx}^1(\lambda,y)=(1-\nu_1)\bar{\sigma}_0, \qquad y\in[0,h_1)$$
$$\sigma_{xx}^2(\lambda,y)=0, \qquad y\in(h_1,h_1+h_2]$$
$$\sigma_{xy}^i(\lambda,y)=0, \qquad y\in[0,h_1+h_2], \qquad i=1,2 \tag{4}$$

$$\sigma_{xy}^1(x,0)=\sigma_{yy}^1(x,0)=\sigma_{xy}^2(x,h_1+h_2)=\sigma_{yy}^2(x,h_1+h_2)=0 \tag{5}$$

The interfacial continuity at the interface $y=h_1$ requires additional displacement and stress continuity equations, as

$$u_x^1=u_x^2, \qquad u_y^1=u_y^2$$
$$\sigma_{xy}^1=\sigma_{xy}^2, \qquad \sigma_{yy}^1=\sigma_{yy}^2 \tag{6}$$

Based on Saint-Venant's principle, the eccentric applied load $(1-\nu_1)\bar{\sigma}_0$ in Fig. 3 is equivalent to the superposition of a uniform axial stress and a pure bending moment, which can be addressed by classical beam theory. Shear lag also exists between layers, resulting in a shear transfer through the interface. Considering the deformation patterns and their physics, two trial functions were proposed to represent the displacement due to the pure bending and shear transfer as (Kim et al. 2009; Lin et al. 2017)

$$u_x^i=u_x^{bi}+u_x^{si}$$
$$u_y^i=u_y^{bi}+u_y^{si} \tag{7}$$

where b and s = bending and shearing, respectively.

The pure bending part could be easily determined with the help of classical beam theory in the form of

$$u_x^{bi}=\kappa(y-y_{\mathrm{NA}})x$$
$$u_y^{bi}=-\frac{1}{2}\kappa x^2 \tag{8}$$

$$\sigma_{xx}^{bi}=E_i\kappa(y-y_{\mathrm{NA}})$$
$$\sigma_{xy}^{bi}=\sigma_{yy}^{bi}=0 \tag{9}$$

where κ = curvature; and y_{NA} indicates the location of the neutral axis, which is determined by letting the net axial force equal zero

$$y_{\mathrm{NA}}=\frac{E_1h_1^2+E_2h_2^2+2E_2h_1h_2}{2(E_1h_1+E_2h_2)} \tag{10}$$

As for the shear transfer part, the trial function for the horizontal displacement can be written in the following form through the separation of variables (Yin and Prieto-Muñoz 2013):

$$u_x^{si}=X_i(x)Y_i(y)+\bar{\varepsilon}x \tag{11}$$

The shear lag mechanism is mainly caused by deformation mismatch between layers. It is hypothesized that the vertical displacement in the shearing part is only a function of the y-coordinate (Nairn and Mendels 2001) because the horizontal layer keeps plane during the deformation, which is mathematically described as $u_{y,x}^{si}\approx 0$. By combining Eqs. (11) and (2) and eliminating the terms that contain $u_{y,x}^{si}$, the following differential equation is obtained:

$$\frac{X_i''}{X_i}=-\frac{1-\nu_i}{2}\frac{Y_i''}{Y_i}=c^2 \tag{12}$$

With a positive quantity c, Eq. (12) produces two decoupled ordinary differential equations whose general solutions are obtained separately with coefficients A_i, B_i, C_i, and D_i as follows:

$$X_i=C_i\cosh(cx)+D_i\sinh(cx)$$
$$Y_i=A_i\cos(d_iy)+B_i\sin(d_iy) \tag{13}$$

where the parameter d_i is defined for convenience

$$d_i=c\sqrt{\frac{2}{1-\nu_i}} \tag{14}$$

According to the displacement boundary condition $u_x^i(0,y)=0$, the parameter C_i must be zero, and thus the horizontal displacement is simplified as follows:

$$u_x^{si}=F_i\cos[d_i(y-y_i)]\sinh(cx)+\bar{\varepsilon}x \tag{15}$$

The vertical displacement induced by the shearing u_y^{si} has a negligible impact on the total displacement because the bending deflection u_y^{bi} makes the dominant contribution. Therefore, the displacement u_y^{si} and its partial derivative $u_{y,x}^{si}$ were omitted, although they can be derived from Eq. (2). With the approximation $u_{y,x}^{si}\approx 0$ mentioned previously and the fact that a Bernoulli–Euler beam does not produce shear effects, the shear stress can be written in a concise expression as

$$\sigma_{xy}^i=\frac{E_i}{2(1+\nu_i)}u_{x,y}^{si} \tag{16}$$

The parameter y_i in Eq. (15) is obtained by the stress boundary condition in Eq. (5) that $\sigma_{xy}^i=0$ at the free faces

$$\sigma_{xy}^1(x,0)=\frac{E_1}{2(1+\nu_1)}F_1d_1\sin(d_1y_1)\sinh(cx)=0$$
$$\sigma_{xy}^2(x,h_1+h_2)=-\frac{E_2}{2(1+\nu_2)}F_2d_2\sin[d_2(h_1+h_2-y_2)]\sinh(cx)=0 \tag{17}$$

which gives an explicit form of y_i as

$$y_1=0$$
$$y_2=h_1+h_2 \tag{18}$$

The parameters c and d_i introduced in Eqs. (12) and (14) are determined by the interfacial continuity in Eq. (6). From the horizontal displacement and shear stress continuity conditions, the following two independent equations can be obtained:

$$F_1\cos(d_1h_1)=F_2\cos(d_2h_2) \tag{19}$$

$$-\frac{E_1}{1+\nu_1}F_1d_1\sin(d_1h_1)=\frac{E_2}{1+\nu_2}F_2d_2\sin(d_2h_2) \tag{20}$$

A trigonometric function with respect to d_i is thus obtained by dividing Eq. (20) by Eq. (19), as

$$\frac{E_1}{1+\nu_1}d_1\tan(d_1h_1)+\frac{E_2}{1+\nu_2}d_2\tan(d_2h_2)=0 \tag{21}$$

It is seen that the tangent function is included in the equation, indicating an infinite number of solutions. For simplicity, the asymptotic solution is obtained by taking the first term of the

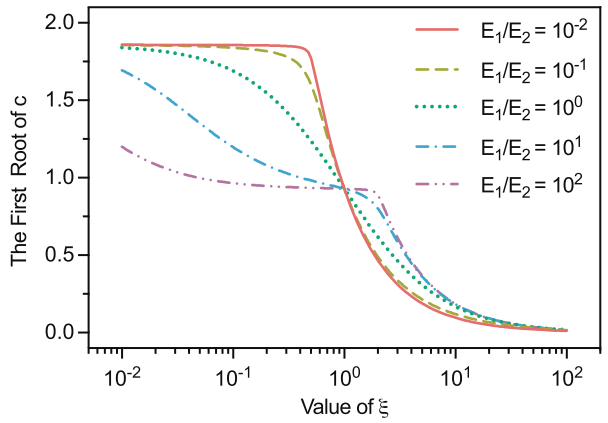

Fig. 4. Relation between the first root of c and parameter ξ with $\nu_1 = \nu_2$ and five stiffness ratios E_1/E_2.

infinite series, with a slight compromise between accuracy and completeness. A dimensionless parameter ξ is widely used to solve for the root of d_i (Yin and Prieto-Muñoz 2013), as

$$\xi = \frac{d_2 h_2}{d_1 h_1} = \frac{h_2}{h_1}\sqrt{\frac{1-\nu_1}{1-\nu_2}} \tag{22}$$

After d_i is determined, the root of c is calculated from Eq. (14). The relations between the first root of c with varying values of ξ under $\nu_1 = \nu_2$ and five stiffness ratios of E_1/E_2 are illustrated in Fig. 4.

Trial functions are derived from the governing equations in Eq. (2), with the parameters c, d_i, and y_i determined by the boundary conditions in Eq. (17) and the interfacial continuity condition in Eq. (21). The following derivation will determine the coefficient of each trial function with the aid of variational principles.

Principle of Stationary Potential Energy

The principle of stationary potential energy is applied to obtain the coefficients of trial functions with the following two assumptions:

- Stress components σ_{xx} and σ_{xy} contribute to the majority of the strain energy, whereas σ_{yy} is neglected due to its minor influence (Yin and Prieto-Muñoz 2013), and
- The boundary effect in the shear-induced part is ignored when calculating the strain energy from the normal stress σ_{xx}.

Therefore, the corresponding stress components σ_{ij}, strain energy U, and work done by the external load W are constructed as

$$\begin{aligned}\sigma_{xx}^i &\approx \sigma_{xx}^{bi} = E_i u_{x,x}^{bi}\\ \sigma_{xy}^i &\approx \frac{E_i}{2(1+\nu_i)} u_{x,y}^{si}\end{aligned} \tag{23}$$

$$\begin{aligned}U = &\frac{1}{2}\int_0^{h_1} \mathrm{d}y \int_{-\lambda}^{\lambda}\left[E_1 (u_{x,x}^1)^2 + \frac{E_1}{2(1+\nu_1)}(u_{x,y}^1 + u_{y,x}^{b1})^2\right]\mathrm{d}x\\ &+\frac{1}{2}\int_{h_1}^{h_1+h_2} \mathrm{d}y \int_{-\lambda}^{\lambda}\left[E_2 (u_{x,x}^2)^2 + \frac{E_2}{2(1+\nu_2)}(u_{x,y}^2 + u_{y,x}^{b2})^2\right]\mathrm{d}x\end{aligned} \tag{24}$$

$$W = 2(1-\nu_1)\bar{\sigma}_0 \int_0^{h_1} u_x^1(\lambda, y)\mathrm{d}y \tag{25}$$

Both the strain energy U and work done by the external load W are evaluated with per-unit length in the z-direction. Because the energy is a positive definite quadratic function, the strain energy can be written as

$$U = T_{11}\kappa^2 + 2T_{12}\kappa\bar{\varepsilon} + 2T_{13}\kappa F_1 + T_{22}\bar{\varepsilon}^2 + 2T_{23}\bar{\varepsilon}F_1 + T_{33}F_1^2 \tag{26}$$

where T_{ij} are calculated via Eq. (24)

$$\begin{aligned}T_{11} &= \frac{E_1 h_1 \lambda}{3}(h_1^2 - 3h_1 y_{NA} + 3y_{NA}^2)\\ &\quad + \frac{E_2 h_2 \lambda}{3}(3h_1^2 + 3h_1 h_2 - 6h_1 y_{NA} + h_2^2 - 3h_2 y_{NA} + 3y_{NA}^2)\\ T_{12} &= \frac{E_1 h_1 \lambda}{3}(h_1 - 2y_{NA}) + \frac{E_2 h_2 \lambda}{2}(2h_1 + h_2 - 2y_{NA})\\ T_{13} &= 0\\ T_{22} &= E_1 h_1 \lambda + E_2 h_2 \lambda\\ T_{23} &= 0\\ T_{33} &= \frac{E_1 d_1}{32(1+\nu_1)c}[\sinh(2c\lambda) - 2c\lambda][2d_1 h_1 - \sin(2d_1 h_1)]\\ &\quad + \frac{E_2 d_2 \cos^2(d_1 h_1)}{32(1+\nu_2)c\cos^2(d_2 h_2)}\\ &\quad \times [\sinh(2c\lambda) - 2c\lambda][2d_2 h_2 - \sin(2d_2 h_2)]\end{aligned} \tag{27}$$

Similarly, the work done by the external load is written as

$$W = 2u_1\kappa + 2u_2\bar{\varepsilon} + 2u_3 F_1 \tag{28}$$

where u_i are calculated via Eq. (24)

$$\begin{aligned}u_1 &= \frac{(1-\nu_1)\bar{\sigma}_0 \lambda (h_1^2 - 2h_1 y_{NA})}{2}\\ u_2 &= (1-\nu_1)\bar{\sigma}_0 \lambda h_1\\ u_3 &= \frac{(1-\nu_1)\bar{\sigma}_0 \sinh(c\lambda)\sin(d_1 h_1)}{d_1}\end{aligned} \tag{29}$$

The potential energy Π is defined as $\Pi = U - W$. According to the principle of stationary potential energy, the variation of the potential energy is zero, that is, $\delta\Pi = 0$. Therefore, the unknowns $(\kappa, \bar{\varepsilon}, F_1)$, which are treated as generalized displacements, can be obtained as

$$\begin{Bmatrix}\kappa\\ \bar{\varepsilon}\\ F_1\end{Bmatrix} = \begin{bmatrix}T_{11} & T_{12} & T_{13}\\ T_{13} & T_{22} & T_{23}\\ T_{13} & T_{23} & T_{33}\end{bmatrix}^{-1}\begin{Bmatrix}u_1\\ u_2\\ u_3\end{Bmatrix} \tag{30}$$

where the symmetric property $T_{ij} = T_{ji}$ is ensured due to the quadratic strain energy expression in Eq. (26). As a result, the elastic field can be written in terms of the generalized displacements as follows:

$$\begin{aligned}u_x^i &= \kappa x(y - y_{NA}) + F_i \cos[d_i(y - y_i)]\sinh(cx) + \bar{\varepsilon}x\\ u_y &= -\frac{1}{2}\kappa x^2\end{aligned} \tag{31}$$

$$\begin{aligned}\sigma_{xx}^i &= E_i\kappa(y - y_{NA}) + E_i F_i c\cos[d_i(y - y_i)]\cosh cx + E_i\bar{\varepsilon}\\ \sigma_{xy}^i &= -\frac{E_i}{2(1+\nu_i)}F_i d_i \sin[d_i(y - y_i)]\sinh cx\end{aligned} \tag{32}$$

Table 1. Geometric details in the FEM verification

Load case	h_1 (mm)	h_2 (mm)	λ (mm)
Case I	3	0.5	600
Case II	6	0.5	600

Table 2. Material properties in the FEM verification

Layer number	Young's modulus (GPa)	Poisson's ratio	External load (MPa)	Thermal expansion coefficients (K^{-1})
Layer 1	72	0.28	9.36	8.8×10^{-6}
Layer 2	190	0.20	0	3.6×10^{-6}

Numerical Verification

The theoretical formulation was verified by FEM analysis conducted in ABAQUS version R2019x. An overlay-substrate model was constructed with the geometric and material properties listed in Tables 1 and 2, respectively. A plane stress model was established with the biquadratic quadrilateral element CPS8. The element size used in each load case was approximately 0.2×0.2 mm so as to guarantee at least 18 elements along the depth direction. The temperature difference was prescribed at $\Delta T = 25$ K, and the corresponding thermal load was therefore calculated as $(1 - \nu_1)\bar{\sigma}_0 = 9.36$ MPa with the help of Eq. (1). The displacement boundary conditions were applied in accordance with Eq. (3). In postprocessing, displacements and stresses were extracted and averaged on the nodes.

The proposed model was compared with FEM results and other analytical models, including Stoney's equation (Stoney 1909), the Yin-Muñoz model (Yin and Prieto-Muñoz 2013), and the Suhir model (Suhir 1988). The Yin-Muñoz model falls into the category of shear lag theory, which is based on the fully bonded interface assumption. Nevertheless, it cannot capture bending deformation. The Suhir model, on the contrary, considers both bending and shear at the interface as a one-dimensional problem, but it cannot predict the shear stress variation along the depth direction. Both the Yin Munoz and Suhir models were used to compare the stress components σ_{xx} and σ_{xy}, whereas Stoney's equation was used to compare the bending displacements u_x and u_y.

The horizontal displacements u_x at the top surface, interface, and bottom surface were extracted from both the proposed analytical model and FEM results. The comparisons were plotted in Figs. 5(a) and 6(a) for Cases I and II, respectively. The vertical displacements u_y were compared among the proposed analytical model, Stoney's equation, modified Stoney's equation (Freund et al. 1999), and FEM results in Figs. 5(b) and 6(b) for Cases I and II, respectively. It was seen that the proposed model converged to the modified Stoney's equation with high accuracy because those two theories consider the strain energy stored in the overlay, which is not considered in the original Stoney model. The comparisons of the normal stress σ_{xx} among the proposed analytical model, Yin-Muñoz model, and FEM results are demonstrated in Figs. 5(c) and 6(c). Because the Yin-Muñoz model neglects pure bending, the flexural stress is not

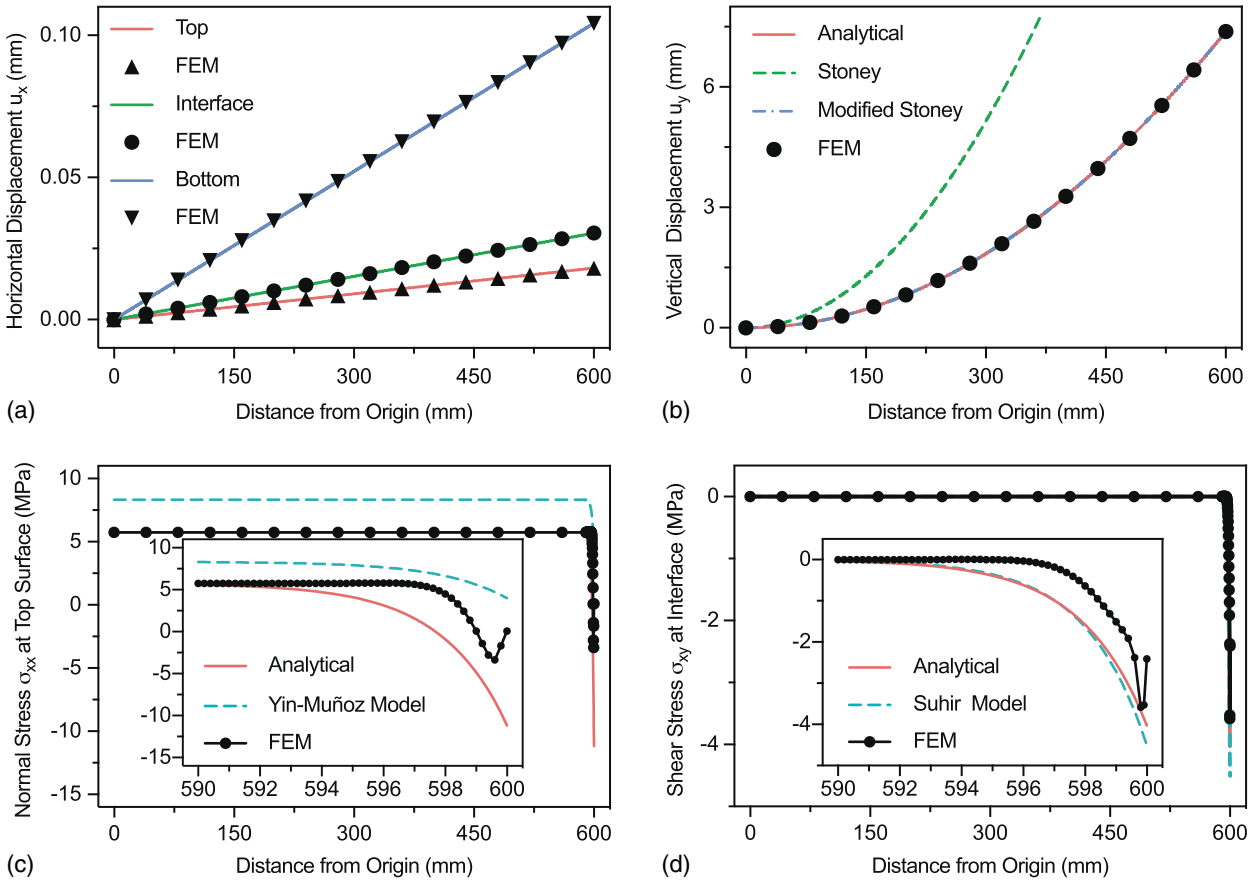

Fig. 5. Comparison between theoretical models and FEM results in load Case I: (a) horizontal displacement u_x with varying distance from origin; (b) vertical displacement u_y with varying distance from origin; (c) normal stress σ_{xx} at top surface with varying distance from origin; and (d) shear stress σ_{xy} at interface with varying distance from origin.

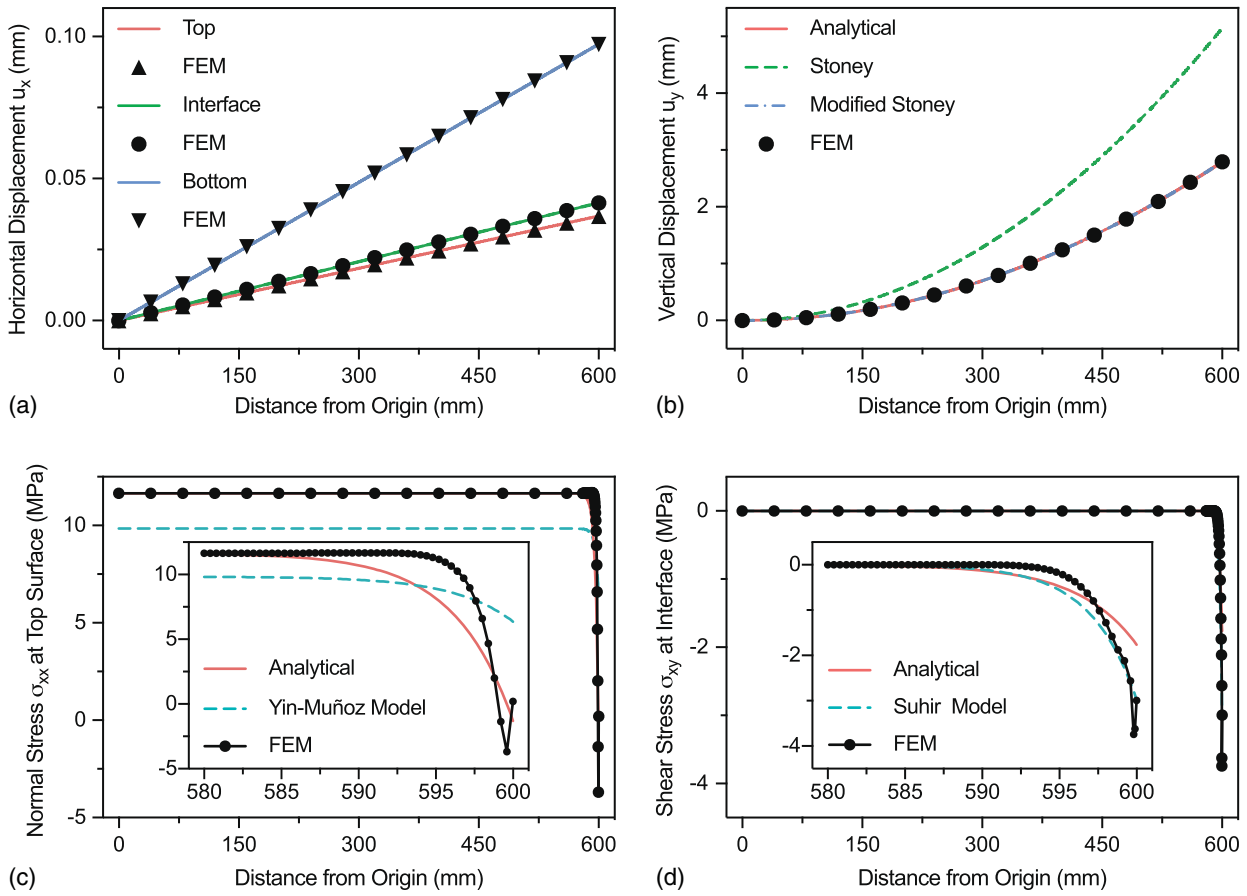

Fig. 6. Comparison between theoretical models and FEM results in load Case II: (a) horizontal displacement u_x with varying distance from origin; (b) vertical displacement u_y with varying distance from origin; (c) normal stress σ_{xx} at top surface with varying distance from origin; and (d) shear stress σ_{xy} at interface with varying distance from origin.

reflected in the normal stress σ_{xx} prediction. Therefore, curvature is necessary to accurately calculate the normal stress σ_{xx}. The comparisons of the shear stress σ_{xy} among the proposed analytical model, Suhir model (Suhir 1988), and FEM results are demonstrated in Figs. 5(d) and 6(d), which validates the argument that the shear stress is only significant close to the end, serving as a corrective solution to explain the boundary effects. Nevertheless, the shear stress at the endpoint $\sigma^i_{xy}(\lambda, y)$ given by the FEM results appears incompatible with the boundary conditions prescribed in Eq. (4). Herein, two possible reasons are presented to account for this phenomenon. First, the displacement-based FEM possesses an intrinsic feature such that stresses have lower accuracy and a slower rate of convergence than displacements. Second, the material discontinuity at the interface makes it difficult for the FEM to converge to the assigned stress boundary conditions, even with a refined mesh and higher-order elements. This incompatibility, as a weakness of FEM results, has been extensively noted and conceded in the literature (Yin and Prieto-Muñoz 2013; Li et al. 2018).

Overall, the present formulation provided very good agreement with high-fidelity FEM results in terms of displacement, and it can capture both bending and shearing effects with advantages over the pure bending or shear lag models, although it exhibits discrepancies when calculating the shear stress around the endpoint due to the singular effect by the material mismatch (Bogy 1968). Displacements have higher accuracy than shear stress functions. This phenomenon is explained by the fact that the primary deformation pattern is well explained by the pure bending trial functions in most regions. Therefore, the local variation of the stress transfer at the endpoint does not significantly influence the displacement. Because Saint-Venant's principle and bending and shearing assumptions were adopted in the present formulation, it cannot illustrate the singularity shown in the FEM results. Moreover, the formulation only contains the first term of the series solutions in Eq. (21), so the closed-form solution may also produce inaccuracy if convergence is not achieved efficiently.

Discussion and Parametric Analysis

Remarks on Model Selection

Several models were introduced and compared in the previous section. Each model has its scope of application according to specific assumptions and approximations. Although our proposed model is versatile in dealing with various cases, other models can be adopted for calculation convenience. Some remarks on the model selection are presented as follows:

- In a thin film or substrate structure, Stoney's equation is able to capture the curvature under a mismatch stress, whereas the shear stress cannot be analyzed;
- In a thin film or substrate structure, shear stress can be calculated via the Suhir and Yin-Muñoz models. The Suhir model has a concise form to consider both bending and shearing effects, but it ignores cross sectional shear lag. The Yin-Muñoz model, which focuses on shear lag, neglects bending curvature so that normal stress accuracy will be compromised; and

J. Eng. Mech., 2021, 147(7): 04021034

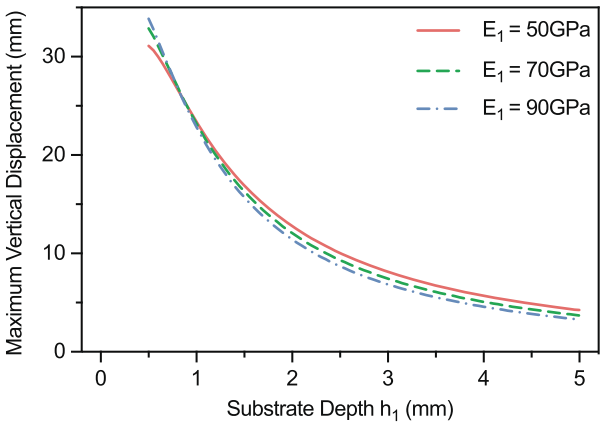

Fig. 7. Maximum vertical displacement u_y with varying substrate depth h_1 under three different E_1 values.

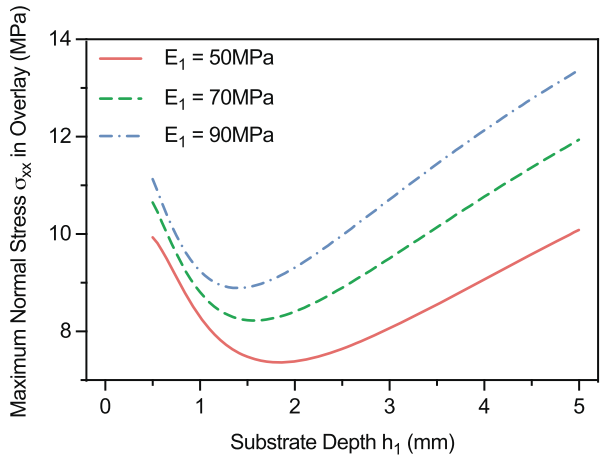

Fig. 8. Maximum normal stress σ_{xx} in the overlay with varying substrate depth h_1 under three different E_1 values.

- In a general overlay or substrate structure, the modified Stoney's equation is able to accurately address curvature but cannot deal with shear stress.

Our proposed model applies to each situation mentioned previously due to the fact that it generalizes and unifies the modified Stoney's equation and Yin-Muñoz model, whose limitations are thus eliminated.

Parametric Study

As a structural member, the substrate has a significant impact on the displacement and stress distributions in the overlay–substrate system. A parametric study was conducted to quantify the effect of material stiffness and substrate depth on the thermomechanical performance of the structure, aiming for a more efficient substrate design. Both overlay and substrate have the geometries and material properties given in Tables 1 and 2, except that Young's modulus E_1 and depth of the substrate h_1 are taken as two variables in our parametric study. Numerical results are shown subsequently to illustrate the maximum vertical displacement u_y, maximum tensile stress σ_{xx} in the overlay, and maximum shear stress σ_{xy} along the interface,

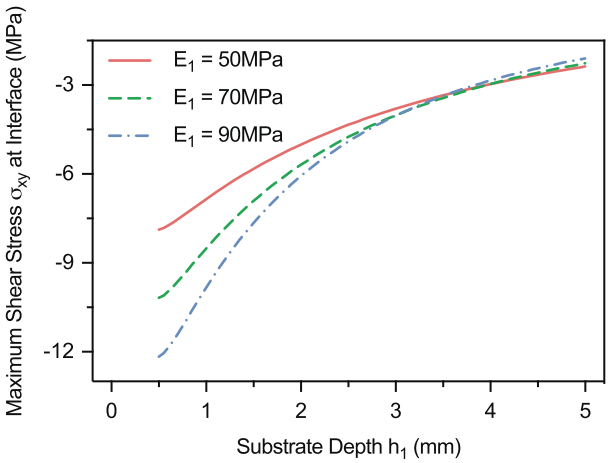

Fig. 9. Maximum shear stress σ_{xy} on the interface with varying substrate depth h_1 under three different E_1 values.

with varying substrate depth h_1 and three different substrate Young's modulus values E_1.

It is observed in Fig. 7 that using the substrate with a high Young's modulus E_1 does not effectively reduce the thermomechanical deflection of the layered structure, which is because the external load $\bar{\sigma}_0$ becomes larger with the increase of Young's modulus E_1, as indicated in Eq. (1). Thus, the stiffness of the substrate is not sensitive in the design, whereas the depth of the substrate plays a more critical role. As illustrated in Fig. 8, the proper depth of the substrate can minimize the normal stress σ_{xx} in the overlay so as to avoid fracture and failure. With the increase of substrate depth, the shear stress σ_{xy} at the interface decreases to a converged value so that delamination and sliding can be avoided, as indicated in Fig. 9.

Conclusions

This paper presents a unified theory that captures the bending and shearing effects of a bilayered composite under a uniform temperature change. It serves as a generalized version of Stoney's equation with particular consideration for shear transfer. Bending and shearing effects were addressed by two admissible trial functions with the help of separation of variables. Boundary conditions and interfacial continuity are discussed and were used to determine the unknown parameters. The coefficients corresponding to the bending and shearing trial functions were determined through the principle of stationary potential energy. Good agreement was achieved between the analytical solutions and FEM results, which demonstrates the accuracy of the proposed model. However, because of Saint-Venant's principle and prescribed assumptions, the present formulation cannot capture the singularity at the end of the interface. The proposed model is suitably considered as a simple but effective approach to aid engineers in conducting rapid iterative design for optimal structural parameters. It is also a robust algorithm that could be easily extended to multilayered composites.

Appendix. Plane Stress Assumption Verification

In order to verify the assumptions of the proposed methodology, FEM simulations are described in this section, where the proposed two-dimensional (2D) plane stress model was compared to a 3D model in ABAQUS. The dimensions of the 3D model were $2L_x = 20$ m, $L_y = 1$ m, and $2L_z = 2$ m, and the 2D model ignored the

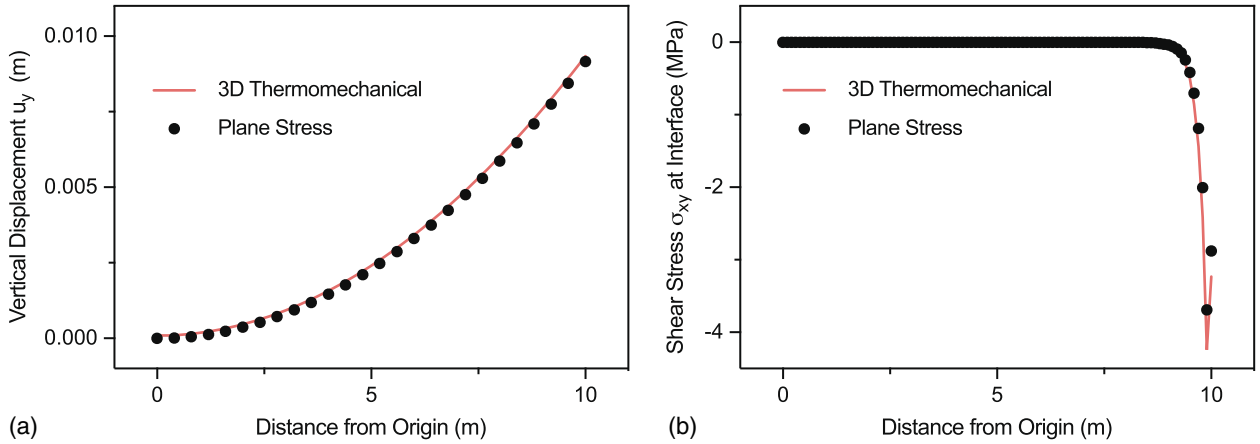

Fig. 10. Comparisons between 3D thermomechanical and 2D plane stress models: (a) vertical displacement u_y; and (b) shear stress σ_{xy}.

depth in the L_z-direction. Without loss of generality, the two layers were assumed to be the same thickness $L_y/2$ and attached along the y-direction. Thanks to symmetry, one-quarter of the 3D model and one-half of the 2D model were analyzed with nonnegative values of $x \in [0, L_x]$ and $z \in [0, L_z]$. The material properties are given in Table 2. The 3D model was meshed with $0.1 \times 0.1 \times 0.1$ m quadratic hexahedral C3D20 elements, whereas the 2D model was meshed with 0.1×0.1 m quadratic quadrilateral CPS8 elements. The temperature change $\Delta T = 25$ K was imposed as a thermal load in the 3D thermomechanical analysis, with $u_x(0, y, z) = 0$, $u_y(0, L_y/2, z) = 0$, and $u_z(x, y, 0) = 0$ prescribed as the displacement boundary conditions. The corresponding thermal mismatch stress $(1 - \nu_1)\bar{\sigma}_0 = E_1(\alpha_1 - \alpha_2)\Delta T = 9.36$ MPa was applied in the 2D plane stress model as a stress boundary condition, with $u_x(0, y) = 0$ and $u_y(0, L_y) = 0$ prescribed as the displacement boundary conditions.

In the 3D model, displacement and shear stress were extracted and averaged from nodes $(x, L_y/2, 0)$, which is the intersection line of the interface and symmetry plane xy at $z = 0$. In the 2D model, displacement and shear stress were extracted and averaged from nodes on the interface $(x, L_y/2)$. The comparisons are illustrated in Figs. 10(a and b), respectively. Almost identical distributions were observed in both comparisons, which verifies the accuracy of the proposed plane stress model when the z-dimension is much smaller than the x-dimension. However, as the z-dimension increases, the results of the proposed plane stress theory will gradually deviate from the 3D case, and plate theory will be necessary to address the behavior.

Data Availability Statement

Some data, models, or codes that support the findings of this study are available from the corresponding author upon reasonable request, including the finite-element model and results, as well as the numerical data for comparisons with other previous models.

Acknowledgments

This work is sponsored by the National Science Foundation IIP #1738802 and CMMI#1762891, whose support is gratefully acknowledged.

References

Anbusagar, N. R. R., K. Palanikumar, and P. K. Giridharan. 2015. "Study of sandwich effect on nanoclay modified polyester resin GFR face sheet laminates." *Compos. Struct.* 125 (Jul): 336–342. https://doi.org/10.1016/j.compstruct.2015.02.016.

Bogy, D. B. 1968. "Edge-bonded dissimilar orthogonal elastic wedges under normal and shear loading." *J. Appl. Mech.* 35 (3): 460–466. https://doi.org/10.1115/1.3601236.

Chen, F. L., X. He, P. A. Prieto-Muñoz, and H. M. Yin. 2015. "Opening-mode fractures of a brittle coating bonded to an elasto-plastic substrate." *Int. J. Plast.* 67 (Apr): 171–191. https://doi.org/10.1016/j.ijplas.2014.10.007.

Corkovic, S., R. W. Whatmore, and Q. Zhang. 2008. "Development of residual stress in sol-gel derived Pb(Zr, Ti)O_3 films: An experimental study." *J. Appl. Phys.* 103 (8): 084101. https://doi.org/10.1063/1.2890142.

Feng, X., Y. Huang, H. Jiang, D. Ngo, and A. J. Rosakis. 2006. "The effect of thin film/substrate radii on the Stoney formula for thin film/substrate subjected to nonuniform axisymmetric misfit strain and temperature." *J. Mech. Mater. Struct.* 1 (6): 1041–1053. https://doi.org/10.2140/jomms.2006.1.1041.

Freund, L. B., J. A. Floro, and E. Chason. 1999. "Extensions of the Stoney formula for substrate curvature to configurations with thin substrates or large deformations." *Appl. Phys. Lett.* 74 (14): 1987–1989. https://doi.org/10.1063/1.123722.

Guo, L., and S. P. DeWeerth. 2010. "High-density stretchable electronics: Toward an integrated multilayer composite." *Adv. Mater.* 22 (36): 4030–4033. https://doi.org/10.1002/adma.201000515.

Haftbaradaran, H., S. K. Soni, B. W. Sheldon, X. Xiao, and H. Gao. 2012. "Modified Stoney equation for patterned thin film electrodes on substrates in the presence of interfacial sliding." *J. Appl. Mech.* 79 (3): 031018. https://doi.org/10.1115/1.4005900.

Hou, S., C. Shu, S. Zhao, T. Liu, X. Han, and Q. Li. 2015. "Experimental and numerical studies on multi-layered corrugated sandwich panels under crushing loading." *Compos. Struct.* 126 (Aug): 371–385. https://doi.org/10.1016/j.compstruct.2015.02.039.

Huang, S., and X. Zhang. 2006. "Extension of the Stoney formula for film–substrate systems with gradient stress for MEMS applications." *J. Micromech. Microeng.* 16 (2): 382–389. https://doi.org/10.1088/0960-1317/16/2/024.

Kim, S.-E., H.-T. Thai, and J. Lee. 2009. "A two variable refined plate theory for laminated composite plates." *Compos. Struct.* 89 (2): 197–205. https://doi.org/10.1016/j.compstruct.2008.07.017.

Lee, Y. Y., E. W. M. Lee, and C. F. Ng. 2005. "Sound absorption of a finite flexible micro-perforated panel backed by an air cavity." *J. Sound Vib.* 287 (1): 227–243. https://doi.org/10.1016/j.jsv.2004.11.024.

Li, L.-A., R.-J. Li, S.-B. Wang, Z.-Y. Wang, T. Li, and C.-W. Li. 2018. "Stress analysis of film-on-substrate structure under tensile loads." *Mech. Mater.* 120 (May): 1–14. https://doi.org/10.1016/j.mechmat.2018.02.003.

Lin, Q., F. Chen, and H. Yin. 2017. "Experimental and theoretical investigation of the thermo-mechanical deformation of a functionally graded panel." *Eng. Struct.* 138 (May): 17–26. https://doi.org/10.1016/j.engstruct.2017.01.062.

Lin, Q., Y. Zhang, A. Van Mieghem, Y.-C. Chen, N. Yu, Y. Yang, and H. Yin. 2020. "Design and experiment of a sun-powered smart building envelope with automatic control." *Energy Build.* 223 (Sep): 110173. https://doi.org/10.1016/j.enbuild.2020.110173.

MacDonald, W. A., M. K. Looney, D. MacKerron, R. Eveson, R. Adam, K. Hashimoto, and K. Rakos. 2007. "Latest advances in substrates for flexible electronics." *J. Soc. Inf. Disp.* 15 (12): 1075–1083. https://doi.org/10.1889/1.2825093.

Nairn, J. A., and D. A. Mendels. 2001. "On the use of planar shear-lag methods for stress-transfer analysis of multilayered composites." *Mech. Mater.* 33 (6): 335–362. https://doi.org/10.1016/S0167-6636(01)00056-4.

Prieto-Muñoz, P. A., H. M. Yin, and W. G. Buttlar. 2013. "Two-dimensional stress analysis of low-temperature cracking in asphalt overlay/substrate systems." *J. Mater. Civ. Eng.* 25 (9): 1228–1238. https://doi.org/10.1061/(ASCE)MT.1943-5533.0000716.

Razeghi, M. 2002. "Short-wavelength solar-blind detectors-status, prospects, and markets." *Proc. IEEE* 90 (6): 1006–1014. https://doi.org/10.1109/JPROC.2002.1021565.

Roy, R., D. K. Agrawal, and H. A. McKinstry. 1989. "Very low thermal expansion coefficient materials." *Annu. Rev. Mater. Sci.* 19 (1): 59–81. https://doi.org/10.1146/annurev.ms.19.080189.000423.

Stoney, G. G. 1909. "The tension of metallic films deposited by electrolysis." *Proc. R. Soc. London, Ser. A* 82 (553): 172–175. https://doi.org/10.1098/rspa.1909.0021.

Suhir, E. 1988. "An approximate analysis of stresses in multilayered elastic thin films." *J. Appl. Mech.* 55 (1): 143–148. https://doi.org/10.1115/1.3173620.

Sumitomo, T., H. Huang, L. Zhou, and J. Shimizu. 2011. "Nanogrinding of multi-layered thin film amorphous Si solar panels." *Int. J. Mach. Tools Manuf.* 51 (10): 797–805. https://doi.org/10.1016/j.ijmachtools.2011.07.001.

Timm, D. H., B. B. Guzina, and V. R. Voller. 2003. "Prediction of thermal crack spacing." *Int. J. Solids Struct.* 40 (1): 125–142. https://doi.org/10.1016/S0020-7683(02)00496-1.

Yang, D. J., Z. F. Yuan, P. H. Lee, and H. M. Yin. 2012. "Simulation and experimental validation of heat transfer in a novel hybrid solar panel." *Int. J. Heat Mass Transfer* 55 (4): 1076–1082. https://doi.org/10.1016/j.ijheatmasstransfer.2011.10.003.

Yang, Q., B. Zheng, K. Zhang, and J. Zhu. 2013. "Analytical solution of a bilayer functionally graded cantilever beam with concentrated loads." *Arch. Appl. Mech.* 83 (3): 455–466. https://doi.org/10.1007/s00419-012-0693-6.

Yim, W. M., and R. J. Paff. 1974. "Thermal expansion of AlN, sapphire, and silicon." *J. Appl. Phys.* 45 (3): 1456–1457. https://doi.org/10.1063/1.1663432.

Yin, H. M., W. G. Buttlar, and G. H. Paulino. 2007. "Simplified solution for periodic thermal discontinuities in asphalt overlays bonded to rigid pavements." *J. Transp. Eng.* 133 (1): 39–46. https://doi.org/10.1061/(ASCE)0733-947X(2007)133:1(39).

Yin, H. M., and P. A. Prieto-Muñoz. 2013. "Stress transfer through fully bonded interface of layered materials." *Mech. Mater.* 62 (Aug): 69–79. https://doi.org/10.1016/j.mechmat.2013.03.007.

Yin, H. M., D. J. Yang, G. Kelly, and J. Garant. 2013. "Design and performance of a novel building integrated PV/thermal system for energy efficiency of buildings." *Sol. Energy* 87 (Jan): 184–195. https://doi.org/10.1016/j.solener.2012.10.022.

Zhao, Z. B., J. Hershberger, S. M. Yalisove, and J. C. Bilello. 2002. "Determination of residual stress in thin films: A comparative study of X-ray topography versus laser curvature method." *Thin Solid Films* 415 (1): 21–31. https://doi.org/10.1016/S0040-6090(02)00489-3.

Zulkifli, R., J. Mohd Nor, M. F. Mat Tahir, A. R. Ismail, and M. Nuawi. 2008. "Acoustic properties of multi-layer coir fibres sound absorption panel." *J. Appl. Sci.* 8 (20): 3709–3714. https://doi.org/10.3923/jas.2008.3709.3714.